AMERICAN SOCIETY FOR MICROBIOLOGY | Journal of Virology

Homology-Based Identification of a Mutation in the Coronavirus RNA-Dependent RNA Polymerase That Confers Resistance to Multiple Mutagens

Nicole R. Sexton,[a,b] Everett Clinton Smith,[b,c] Hervé Blanc,[d] Marco Vignuzzi,[d] Olve B. Peersen,[e] Mark R. Denison[a,b,c]

Department of Pathology, Microbiology, and Immunology,[a] Department of Pediatrics,[b] and Elizabeth B. Lamb Center for Pediatric Research,[c] Vanderbilt University Medical Center, Nashville, Tennessee, USA; Institut Pasteur, Centre National de la Recherche Scientifique UMR 3569, Paris, France[d]; Department of Biochemistry and Molecular Biology, Colorado State University, Fort Collins, Colorado, USA[e]

ABSTRACT

Positive-sense RNA viruses encode RNA-dependent RNA polymerases (RdRps) essential for genomic replication. With the exception of the large nidoviruses, such as coronaviruses (CoVs), RNA viruses lack proofreading and thus are dependent on RdRps to control nucleotide selectivity and fidelity. CoVs encode a proofreading exonuclease in nonstructural protein 14 (nsp14-ExoN), which confers a greater-than-10-fold increase in fidelity compared to other RNA viruses. It is unknown to what extent the CoV polymerase (nsp12-RdRp) participates in replication fidelity. We sought to determine whether homology modeling could identify putative determinants of nucleotide selectivity and fidelity in CoV RdRps. We modeled the CoV murine hepatitis virus (MHV) nsp12-RdRp structure and superimposed it on solved picornaviral RdRp structures. Fidelity-altering mutations previously identified in coxsackie virus B3 (CVB3) were mapped onto the nsp12-RdRp model structure and then engineered into the MHV genome with [nsp14-ExoN(+)] or without [nsp14-ExoN(−)] ExoN activity. Using this method, we identified two mutations conferring resistance to the mutagen 5-fluorouracil (5-FU): nsp12-M611F and nsp12-V553I. For nsp12-V553I, we also demonstrate resistance to the mutagen 5-azacytidine (5-AZC) and decreased accumulation of mutations. Resistance to 5-FU, and a decreased number of genomic mutations, was effectively masked by nsp14-ExoN proofreading activity. These results indicate that nsp12-RdRp likely functions in fidelity regulation and that, despite low sequence conservation, some determinants of RdRp nucleotide selectivity are conserved across RNA viruses. The results also indicate that, with regard to nucleotide selectivity, nsp14-ExoN is epistatic to nsp12-RdRp, consistent with its proposed role in a multiprotein replicase-proofreading complex.

IMPORTANCE

RNA viruses have evolutionarily fine-tuned replication fidelity to balance requirements for genetic stability and diversity. Responsibility for replication fidelity in RNA viruses has been attributed to the RNA-dependent RNA polymerases, with mutations in RdRps for multiple RNA viruses shown to alter fidelity and attenuate virus replication and virulence. Coronaviruses (CoVs) are the only known RNA viruses to encode a proofreading exonuclease (nsp14-ExoN), as well as other replicase proteins involved in regulation of fidelity. This report shows that the CoV RdRp (nsp12) likely functions in replication fidelity; that residue determinants of CoV RdRp nucleotide selectivity map to similar structural regions of other, unrelated RNA viral polymerases; and that for CoVs, the proofreading activity of the nsp14-ExoN is epistatic to the function of the RdRp in fidelity.

RNA virus replication results in the incorporation of a relatively high number of mutations, ranging from 10^{-4} to 10^{-6} mutations per site per round of replication (1–5). It is thought that low-fidelity replication is largely responsible for the capacity of RNA viruses to evolve rapidly and adapt to new host species and ever-changing environmental pressures (6–8). RNA-dependent RNA polymerase (RdRp) is central to the replication of RNA viruses and is a key regulator of nucleotide selectivity and fidelity (9, 10). Recent studies of coxsackievirus virus B3 (CVB3), poliovirus, HIV-1, and other viruses have demonstrated that viable viruses are recoverable only within a 4-fold range of RdRp fidelity (11–14). In most cases, altered RdRp fidelity decreases fitness relative to wild-type (WT) viruses; this has been demonstrated for changes as small as a 1.2-fold difference in the accumulation of mutations (12, 14–16). Despite having as little as no amino acid identity outside conserved motifs (11–14, 17–19), all described polymerase structures (including RdRps) resemble a "cupped right hand," with finger, palm, and thumb domains (20). The fingers form a channel that allows entry of the template RNA and ribonucleotide triphosphates (rNTPs) and assist in proper positioning of incoming nucleotides in the active site (21). The palm contains the active site, and the thumb functions in contacting exiting nascent RNA (21–23). However, there is diversity in the viral genes that encode RdRps; additional domains that perform a variety of functions, such as methyltransferase, endonuclease, polyribonucleotidyl transferase, guanylyltransferase, membrane targeting, protein-

Received 11 January 2016 **Accepted** 27 May 2016

Accepted manuscript posted online 8 June 2016

Citation Sexton NR, Smith EC, Blanc H, Vignuzzi M, Peersen OB, Denison MR. 2016. Homology-based identification of a mutation in the coronavirus RNA-dependent RNA polymerase that confers resistance to multiple mutagens. J Virol 90:7415–7428. doi:10.1128/JVI.00080-16.

Editor: S. Perlman, University of Iowa

Address correspondence to Mark R. Denison, mark.denison@vanderbilt.edu.

protein binding, or protein-RNA binding activities, are often present (24–26).

Coronaviruses (CoVs) infect a wide array of species and have emerged as highly pathogenic human pathogens twice in this century, first with severe acute respiratory syndrome coronavirus (SARS-CoV) in 2003 (27) and then with Middle East respiratory syndrome coronavirus (MERS-CoV) in 2012 (28). CoVs, and other large nidoviruses, replicate with higher fidelity than all other known positive-sense RNA viruses (29, 30). CoVs also have the largest known RNA virus genomes, ranging from 27 to 34 kb (31, 32), and increased fidelity in CoVs is likely required for the maintenance of these large genomes (14). CoV genomes encode 16 nonstructural proteins (nsp1 to nsp16), several of which are known or predicted to function in fidelity regulation, including nsp14-ExoN, a 3′-5′ exoribonuclease, and nsp10, a modulator of nsp14-ExoN activity (33, 34). Mutating the DE of the nsp14-ExoN active site to AA inactivates the exoribonuclease, yielding nsp14-ExoN(−) viruses, and nsp14-ExoN(−) viruses exhibit a greater-than-10-fold increase in mutation frequency (29, 35–37). Recent evidence has demonstrated that nsp14 directly interacts with the CoV RdRp encoded in nsp12 (nsp12-RdRp) (38), but the effect of this interaction on nucleotide selectivity and overall fidelity regulation is not known. There are no solved structures for any CoV nsp12-RdRp, but the presence of conserved RdRp motifs and modeling of the C-terminal half of nsp12 predict an RdRp domain that is structurally similar to those of other RNA viruses (39, 40).

The demonstrated function of nsp14-ExoN in high-fidelity CoV replication raises the questions of whether and how nsp12-RdRp participates in fidelity regulation. We sought to determine whether nsp12-RdRp can modulate nucleotide selectivity independently or in association with the proofreading nsp14 exonuclease. We modeled the RdRp domain of CoV nsp12 on CVB3 and poliovirus polymerase structures and predicted the residues important for fidelity based on prior results from those virus systems. Substitution mutations at these residues were introduced in the isogenic recombinant genome of the β-CoV murine hepatitis virus (MHV-A59). We demonstrate that two of these mutations, nsp12-V553I and nsp12-M611F, confer resistance to the mutagen 5-fluorouracil (5-FU) and that one, nsp12-V553I, also results in resistance to the mutagen 5-azacytidine (5-AZC) and demonstrates decreased accumulation of mutations. Increased mutagen resistance and decreased accumulation of mutations were observed only in viruses with an inactivated ExoN, demonstrating that nsp14-ExoN proofreading activity is epistatic to the nucleotide selectivity of nsp12-RdRp. In this paper, we define epistasis as a situation where the phenotype of one gene or viral protein masks the phenotype of genetic variants of another viral protein. This result is consistent with a primary role for nsp14-ExoN in error recognition and removal. However, introduction of RdRp mutations within the WT MHV background decreased fitness relative to WT. Together, the results suggest that nsp12-RdRp shares common determinants of nucleotide selectivity with RdRps from other RNA virus families. Further, the CoV RdRp has likely evolved to function in cooperation with nsp14-ExoN rather than independently.

MATERIALS AND METHODS

Virus and cell culture. Murine delayed brain tumor (DBT) cells (41) and baby hamster kidney 21 cells expressing the MHV receptor (BHK-R) (42) were maintained at 37°C in Dulbecco's modified Eagle medium (DMEM) (Gibco) supplemented with 10% fetal bovine serum (FBS) (Invitrogen), penicillin, streptomycin (Gibco), and amphotericin B (Corning). The BHK-R cells were further supplemented with 0.8 mg/ml of G418 (Mediatech). All virus work was performed using the recombinant WT MHV strain MHV-A59 (GenBank accession number AY910861 [42]).

Sequence analysis and homology modeling of CoV MHV nsp12-RdRp. The MHV RdRp domain structure was generated with the Phyre2 online program (43) using nsp12 residues 385 to 887, which correspond to the reported SARS-CoV nsp12-RdRp model (40). The structural model was compared to the X-ray crystal structures of CVB3 and poliovirus (Protein Data Bank [PDB] accession numbers 3DDK and 1RA7, respectively) using the Pymol Molecular Graphics System (Schrödinger, LLC). ClustalX multiple-sequence alignments were generated using the program MacVector.

Cloning, recovery, and verification of mutant viruses. Quick-change mutagenesis was used to generate point mutations in individual MHV genome cDNA fragment plasmids using the previously described MHV infectious clone reverse genetics system (42). Mutant viruses were recovered in cocultured BHK-R and DBT cells following electroporation of *in vitro*-transcribed genome RNA in BHK-R cells. All viruses that included nsp14-ExoN(−) mutations were generated using the F fragment previously described (35). Before use in virus recovery, all mutagenized plasmids were fully sequenced (GenHunter Corporation, Nashville, TN) to ensure no additional mutations were introduced. We also sequence verified engineered mutations in recovered viruses. Viruses in the nsp14-ExoN(−) background took between 84 and 96 h to reach around 80% involvement in syncytia for a passage zero (P0) stock, in contrast to viruses in the WT background, which were frozen at 24 to 48 h postinfection (p.i.). P1 working stocks were made by infecting DBT cells at a multiplicity of infection (MOI) of 0.01 and freezing them when 80% were involved in syncytia, approximately 24 h p.i. for WT viruses and 36 h p.i. for nsp14-ExoN(−) viruses (2 or 3 rounds of replication).

Compounds and drug sensitivity studies. 5-FU was obtained from Sigma, and prepared as 200 mM stock solutions in dimethyl sulfoxide (DMSO). 5-AZC was also obtained from Sigma and prepared as 50 mM stock solutions in water. Subconfluent DBT cells were pretreated for 30 min with DMEM with the indicated concentrations of 5-FU or with DMSO, 5-AZC, or medium alone. The treatment was removed, and the inoculum was added and allowed to adsorb for 1 h at 37°C. The inoculum was then removed, and medium with drug or DMSO was returned. Infection proceeded for 24 h for WT or 32 h for nsp14-ExoN(−) viruses, after which the supernatants were acquired and frozen and the titer was determined by plaque assay as previously described (35).

Virus replication and RNA synthesis assays. Subconfluent DBT cell monolayers in triplicate were infected at an MOI of 0.01 PFU/cell. The virus was allowed to adsorb for 30 min, after which the inocula were removed and the cells were washed 2 times with phosphate-buffered saline (PBS), followed by addition of prewarmed medium. For replication kinetics assays, samples were taken at various time points postinfection. Titering was performed by plaque assay, as previously described (35). For analysis of RNA synthesis, total infected-cell RNA was obtained with TRIzol reagent (Invitrogen) at various times postinfection, and two-step reverse transcription-quantitative PCR (RT-qPCR) was performed as previously described (44).

Determination of specific infectivity. Subconfluent DBT cells were pretreated for 30 min with DMEM with the indicated concentration of 5-FU or with DMSO alone. The treatment was removed, and the inoculum was added and allowed to adsorb for 1 h at 37°C. The inoculum was then removed, and medium with drug or DMSO was returned. Infection proceeded for 20 h for WT or 24 h for nsp14-ExoN(−) virus, and then the supernatants were acquired and frozen, and the titer was determined by plaque assay as previously described (35). The supernatants were also used for RNA genome isolation by adding 100 μl supernatant to 900 μl TRIzol reagent (Invitrogen), chloroform extraction by phase separation, and using the aqueous layer in the PureLink Mini RNA kit (Ambion) according

to the manufacturer's protocol. One-step RT-qPCR was performed as described below, and the ratio of PFU to genomes of the supernatant was determined.

One-step RT-qPCR for determining supernatant genome copies for specific infectivity assay. An RNA standard was generated using the MHV A fragment (42) to generate a 931-nucleotide (nt) RNA. First, cDNA was generated by PCR using the following primers: forward, 5′-TAA TACGACTCACTATAGGGGGCTATGTGGATTGTTGTGG-3′, which begins with a T7 promoter, and reverse, 5′-AATTCTTGACAAGCTC AGGC-3′. RNA for the standard curve was then generated using an mMessage mMachine T7 kit (Ambion). An agarose gel with 1% bleach was run, and an ~900-nt band was observed. RNA was purified using an RNeasy minikit (Qiagen). Dilutions of the standard curve were made from 10^3 to 10^8 genome equivalents for use in assays as needed. Primers and probes for one-step RT-qPCR were purchased from BioSearch Tech. The probe was 5′ 6-carboxyfluorescein (FAM) labeled and 3′ black hole quencher 1 (BHQ-1) labeled with the sequence 5′-TTCTGACAACGGC TACACCCAACG-3′ and made up to 5 μM in nuclease-free water. The primers used were forward, 5′-AGAAGGTTACTGGCAACTG-3′, and reverse, 5′-TGTCCACGGCTAAATCAAAC-3′. Reaction mixtures were set up on ice, with enzyme added last. The final volume for reaction mixtures was 20 μl, with 150 nM probe, 900 nM each primer, 2 μl sample RNA, and 10 μl 2× ToughMix one-step low ROX enzyme mix (Quantas) used per reaction. Samples were plated in duplicate and run on the Applied Biosciences 7500 real-time PCR system with the following conditions: 55°C for 10 min, 95°C for 5 min, 95°C for 30 s, and 60°C for 1 min, with the last two steps repeated 40 times. The standard curve was graphed, and the number of genomes per milliliter was determined.

Competitive fitness of mutant viruses. Subconfluent DBT monolayers were coinfected at a total MOI of 0.01 PFU/ml with RdRp mutant viruses in the nsp14-ExoN(−) background and nsp14-ExoN(−) at either a 1:1, 1:9, or 9:1 ratio. When 50 to 70% of the monolayer was involved in syncytia, total RNA was harvested. The RNA was then reverse transcribed using SuperScriptIII (Invitrogen) according to the manufacturer's protocol, and amplicons were generated using primers designed to cover the region including the codons for both the V553 and M611 residues. Amplicons were sent for sequencing, and electopherograms were analyzed using MacVector.

Passage reversion analysis. Triplicate monolayers of subconfluent DBT cells were infected at an initial MOI of 0.01 PFU/ml of nsp12-V553I and nsp12-M611F viruses in both the WT and nsp14-ExoN(−) backgrounds. The viruses were then blind passaged in triplicate for 5 passages. Total RNA was sequenced across a 1.7-kb region of nsp12-RdRp that included both nsp12-RdRp mutations. Electropherograms were analyzed using MacVector.

Preparation of amplicons for deep sequencing of full viral genomes. Subconfluent DBT cells were infected at an MOI of 0.01 PFU/ml with nsp12-V553I or nsp12-M611F in either the WT or nsp14-ExoN(−) background, with nsp14-ExoN(−) alone, or with the WT alone. The infections were allowed to progress for 20 h, and then RNA was isolated. The RNA was reverse transcribed using SuperScriptIII (Invitrogen) according to the manufacturer's protocol, and 12 amplicons were generated to cover the whole genome and processed as described previously (44).

Deep-sequencing sample preparation and analysis. Amplicons were subsequently purified with a nucleospin PCR purification kit (Macherey-Nagel), quantified with PicoGreen, fragmented (Fragmentase), and prepared using the Illumina NextSeq500 Mid Output 150-cycle kit following the standard protocols. Sequences were obtained with an Illumina NextSeq500 machine. Sequencing runs were analyzed using the previously published ViVan bioinformatics pipeline (45). Briefly, the pipeline performed quality filtering, and adaptor cleaning was done using fastq-clipper (http://hannonlab.cshl.edu/fastx_toolkit/index.html). The 150-nt reads were aligned with the reference sequence with a maximum of 2 mismatches per read using BWA (46) and processed using SAMtools (47) to obtain the nucleotide/base calling at each position. The ViVan pipeline then identified statistically significant variants above the background noise due to sequencing error, calculated for each nucleotide site as follows. For each position throughout the viral genome, base identities and their quality scores were gathered. Each variant allele's rate was initially modified according to its covering read qualities based on a maximum-likelihood estimation and tested for significance using a generalized likelihood ratio test. Additionally, an allele confidence interval was calculated for each allele. In order to correct for multiple testing, a Benjamini-Hochberg false-discovery rate of 5% was set. In all experiments, a minimum coverage of 3,000 reads was obtained, and the background error frequency at every nucleotide site was always below 0.0001. For analysis, we use a conservative frequency cutoff of 0.01, consistent with previous studies (48–50).

Statistical analysis. Statistics were applied as described in the figure legends using GraphPad (La Jolla, CA) Prism 6 software. The number of replicates performed for each experiment is similarly provided in each figure legend. Finally, some of the data were normalized to controls; GraphPad Prism 6 software was also used to perform this analysis.

RESULTS

Homology modeling of MHV nsp12-RdRp polymerase core domain predicts putative fidelity determinants. Mutations that alter nucleotide selectivity have been identified across multiple RNA virus RdRps (3, 11, 51–53); however, whether these residues are conserved across virus families is unknown. We sought to determine whether residues within nsp12-RdRp that are structurally homologous to known RNA virus fidelity determinants would have similar effects on nucleotide selectivity when introduced into the MHV background. To do this, we modeled the structure of MHV nsp12-RdRp using Phyre2 software (43). A series of nsp12-RdRp truncations was assessed, and the highest-confidence model was used for further study. This region corresponded to a published model for the SARS nsp12-RdRp (40) and included residues 385 to 887 of the MHV nsp12 protein, referred to here as the RdRp core domain (Fig. 1A and B). Deletion of the CoV-specific domain (residues 1 to 384) and a small C-terminal portion of the thumb domain (residues 888 to 928) was required to establish this high-confidence model (Fig. 1A). The model was resolved by highest-probability similarity to human rhinovirus serotype 14 (PDB ID 1XR5), rabbit hemorrhagic disease virus (PDB ID 1KHV), and enterovirus 71 (EV71) (PDB ID 3N6M). The Phyre2 confidence, i.e., the probability of true homology of the RdRp core domain with these structures, was >99%, while the identity was only 14 to 20%. Having generated a structural model for the MHV nsp12-RdRp core domain, we next sought to predict the residues involved in nucleotide selectivity. The nsp12-RdRp core domain model was aligned with the solved structure of CVB3 (PDB ID 3DDK) using PyMol (Fig. 1C). A series of CVB3 RdRp mutations have been shown to result in decreased fidelity (10, 11, 54). The CVB3 fidelity determinants were compared with the MHV nsp12-RdRp core domain model. Those that aligned well structurally and by amino acid similarity—MHV nsp12-V553, -M611, -W613, -A621, -Y649, and -K794 (Fig. 1)—were further investigated. Finally, the nsp12 amino acid sequences of 27 different α-, β-, and γ-CoVs were aligned, including SARS-CoV and MERS-CoV. All six identified residues were conserved across these CoVs (Fig. 1D). Analyses of similarity and the types of residues in the picornaviruses were then used to determine the specific amino acid changes that would be introduced at the identified MHV residues. The resulting substitution mutations were engineered in

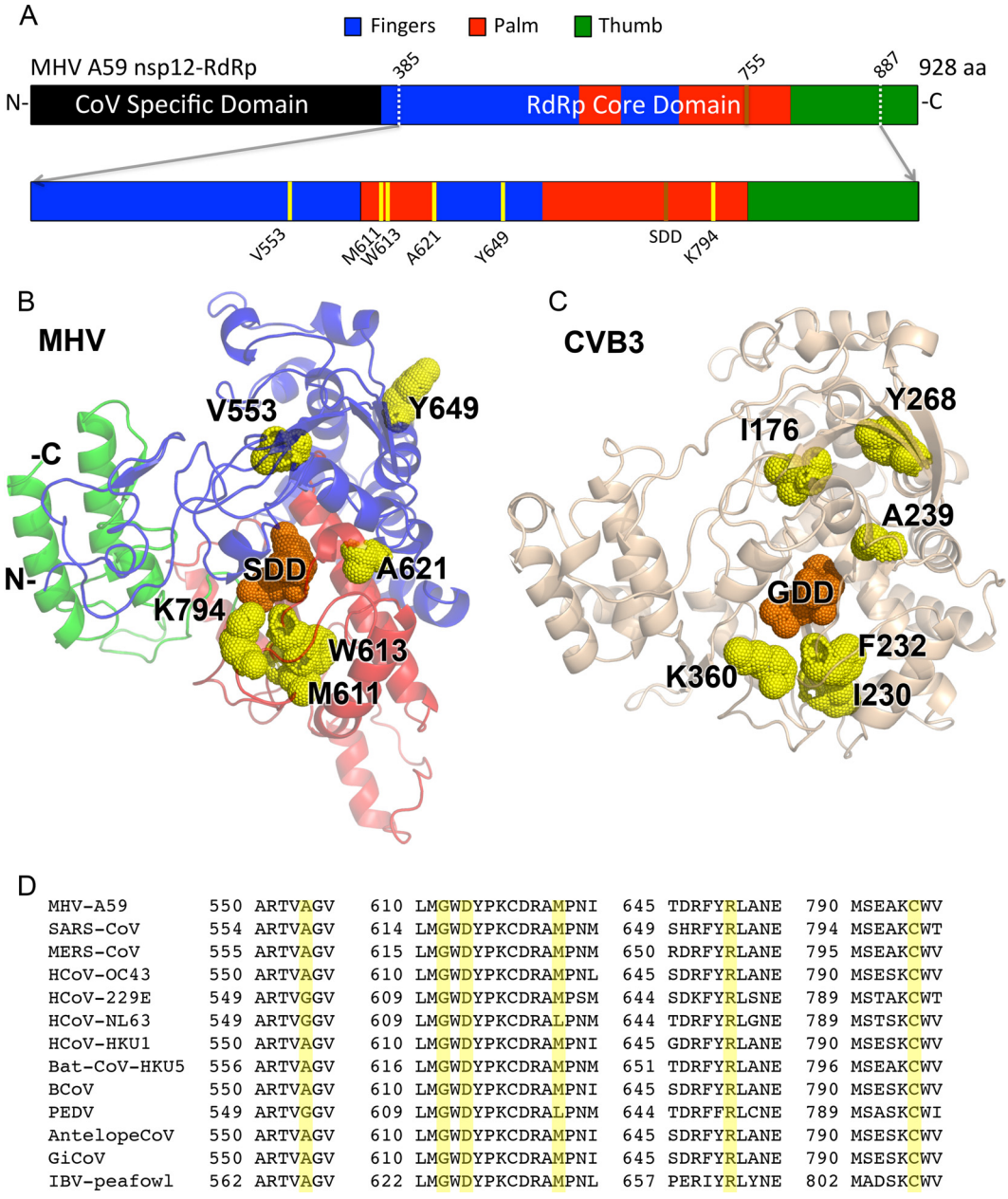

FIG 1 Homology modeling of CoV nsp12-RdRp and identification of residues that potentially regulate fidelity based on CVB3 structure. (A) Phyre2 software was used to model a subsection of the MHV nsp12-RdRp core domain (expanded from the nsp12-RdRp full schematic). (B and C) The modeled MHV RdRp structure (B) was aligned with the solved CVB3 RdRp structure (C). (A and B) The residues chosen for site-directed mutagenesis were selected by comparing previously determined fidelity-altering mutations of picornavirus RdRps. (D) Amino acid alignments across CoVs showing that all residues are almost completely conserved.

the isogenic cloned MHV genome: nsp12-V553A/I, -M611F, -W613Y, -A621G, -Y694H/W, and -K794R (Table 1).

Recovery of mutant viruses in the MHV nsp14-ExoN(+) (with ExoN activity) and nsp14-ExoN(−) isogenic backgrounds. We next tested whether viable viruses could be recovered with substitutions at the identified residues. Virus recovery was attempted a maximum of 3 times, resulting in recovery of 6 of the 8 mutant viruses in the WT background: nsp12-V553I, -M611F, -W613Y, -A621G, -Y649H, and -K794R. The time required for recovery of mutant viruses in the WT background ranged from 24 to 48 h. No other mutations were identified across nsp12 sequences in recovered viruses. The A621G mutant was not further studied, as it demonstrated rapid primary reversion even in the recovery (P0) supernatant. Since our goal was to understand the relationship of nsp12-RdRp and nsp14-ExoN in fidelity regulation, we additionally attempted recovery of the WT background viable mutants in the setting of inactivated nsp14-ExoN [nsp14-ExoN(−)]. In contrast to mutant viruses recovered in the WT background, we recovered only 2 of the 5 mutants in the nsp14-ExoN(−) background: nsp12-V553I/nsp14-ExoN(−) and

TABLE 1 Recovery of mutant viruses using site-directed mutagenesis

nsp12-RdRp region	Engineered substitution (nsp12)		Recovery	
	CVB3[a]	MHV	nsp14-ExoN(+) (WT)	nsp14-ExoN(−)
Fingers	I176V	V553A	No	Not attempted
		V553I	Yes	Yes
	Y268H	Y649H	Yes	No
	Y268W	Y649W	No	Not attempted
Palm	I230F	M611F	Yes	Yes
	F232Y	W613Y	Yes	No
	A239G	A621G	Revertant	Not attempted
	K360R	K794R	Yes	No

[a] Reference 8.

nsp12-M611F/nsp14-ExoN(−) (Table 1). The time to recovery for nsp12-V553I/nsp14-ExoN(−) was 84 h, and that for nsp12-M611F/nsp14-ExoN(−) was 96 h. Working stocks of all the viruses were made by infecting DBT cells at an MOI of 0.01 and recovering stocks at around 24 h p.i. for WT viruses or between 32 and 48 h p.i. for mutant viruses in the nsp14-ExoN(−) background. Therefore, 4 to 10 replication cycles were required to generate stocks. Working stocks were sequenced to verify that the introduced mutations were still present.

Resistance of recovered mutant viruses to the base analog 5-fluorouracil. We next tested our panel of recovered mutant viruses for resistance to the RNA mutagen 5-FU. 5-FU has been used with picornaviruses, influenza viruses, vesicular stomatitis viruses, and others to reflect changes in fidelity based on increased or decreased sensitivity to incorporation and virus inhibition (11, 30, 49, 55). WT CoVs (MHV and SARS-CoV) are resistant to 5-FU, while nsp14-ExoN(−) mutants are profoundly sensitive to 5-FU inhibition, consistent with nsp14-ExoN-mediated removal of misincorporated 5-FU. The effect of 5-FU on DBT cell viability was previously tested, with no effect observed up to 400 μM (30). We compared WT-MHV with the nsp12 mutants in both the WT and nsp14-ExoN(−) backgrounds. There was no significant change in sensitivity to 5-FU compared to WT for any of the nsp12-RdRp mutant viruses in the WT background at up to 120 μM 5-FU, although the mutation Y649H did appear to decrease resistance slightly (Fig. 2A). In contrast, the nsp12-M611F/nsp14-ExoN(−) and nsp12-V553I/nsp14-ExoN(−) mutant viruses were both significantly less sensitive to 5-FU than nsp14-ExoN(−) alone, with both populations persisting when treated with 120 μM 5-FU, where nsp14-ExoN(−) was not detectable beyond 80 μM 5-FU (Fig. 2B). These data demonstrate that both nsp12-RdRp mutations, V553I and M611F, confer resistance to 5-FU. This suggests two possibilities: that it is not possible to increase the exclusion of 5-FU beyond the high level dictated by nsp14-ExoN or that selectivity for native nucleotides over 5-FU is in fact increased by nsp12 mutations, but at a low level that is not detectable as changes in the virus titer.

Three of the mutations (nsp12-Y649H, -W613Y, and -K794R) were viable in the nsp14-ExoN(+) background but failed to grow in the absence of proofreading. The observation that they grew only in an nsp14-ExoN(+) background indicated that the mutations retained sufficient polymerase function to support virus replication but that it was critically dependent on having proofreading functionality, suggesting these mutations may have given rise to low-fidelity variants. Unfortunately, the low titer from the nsp14-ExoN(−) background precluded direct-sequencing analysis, and we therefore cannot definitively show this is the case.

Replication kinetics of nsp12-V553I and nsp12-M611F mutant viruses in the WT and nsp14-ExoN(−) backgrounds. Since we were interested in mutations that potentially confer altered fidelity, we prioritized the nsp12-V553I and nsp12-M611F mutant viruses for further analysis. We next sought to determine how the nsp12-V553I and nsp12-M611F viruses replicated in comparison to their isogenic backgrounds (Fig. 3). In the wild-type background, both mutant viruses had slightly delayed exponential replication but eventually reached similar peak titers comparable to

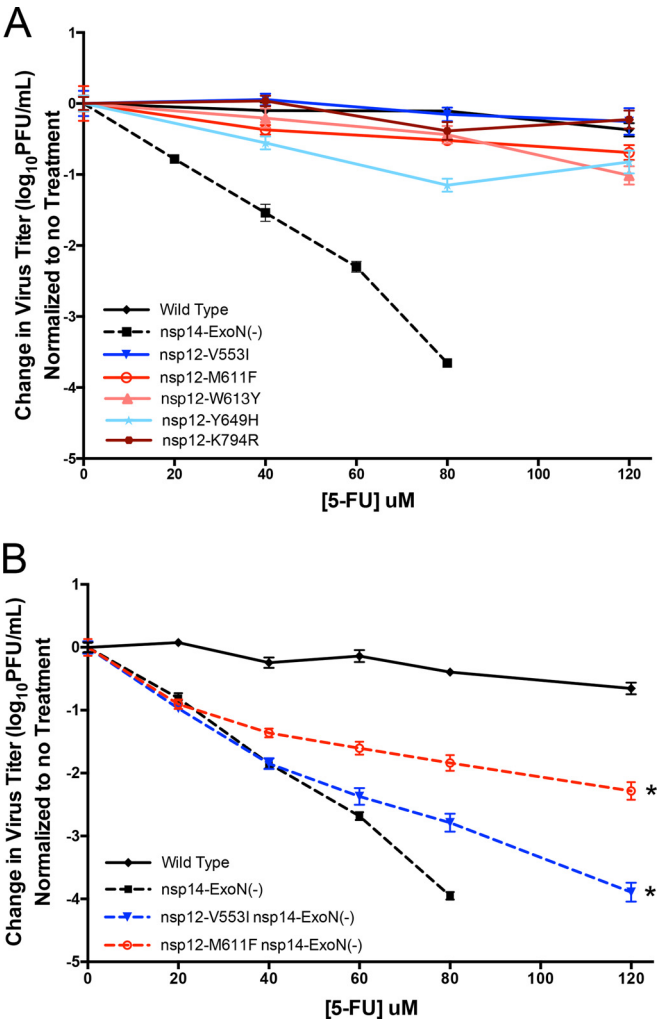

FIG 2 Resistance of MHV nsp12-RdRp mutant viruses to 5-fluorouracil in the WT and nsp14-ExoN(−) backgrounds. The domain locations of mutations are indicated as follows: fingers, blues; palm, reds. DBT cells were pretreated with different concentrations of 5-FU for 30 min. The treatment was removed, and the cells were infected with the indicated viruses in the WT background (A) or the nsp14-ExoN(−) background (B) at an MOI of 0.01. The medium containing 5-FU was replaced 30 min p.i. Virus samples were taken at 24 (WT) or 32 [nsp14-ExoN(−)] h p.i., and the titer was determined by plaque assay. The data represent the results of 3 independent experiments, each with 2 replicates. The error bars represent standard errors of the mean (SEM) *, $P < 0.05$ by the Wilcoxon test.

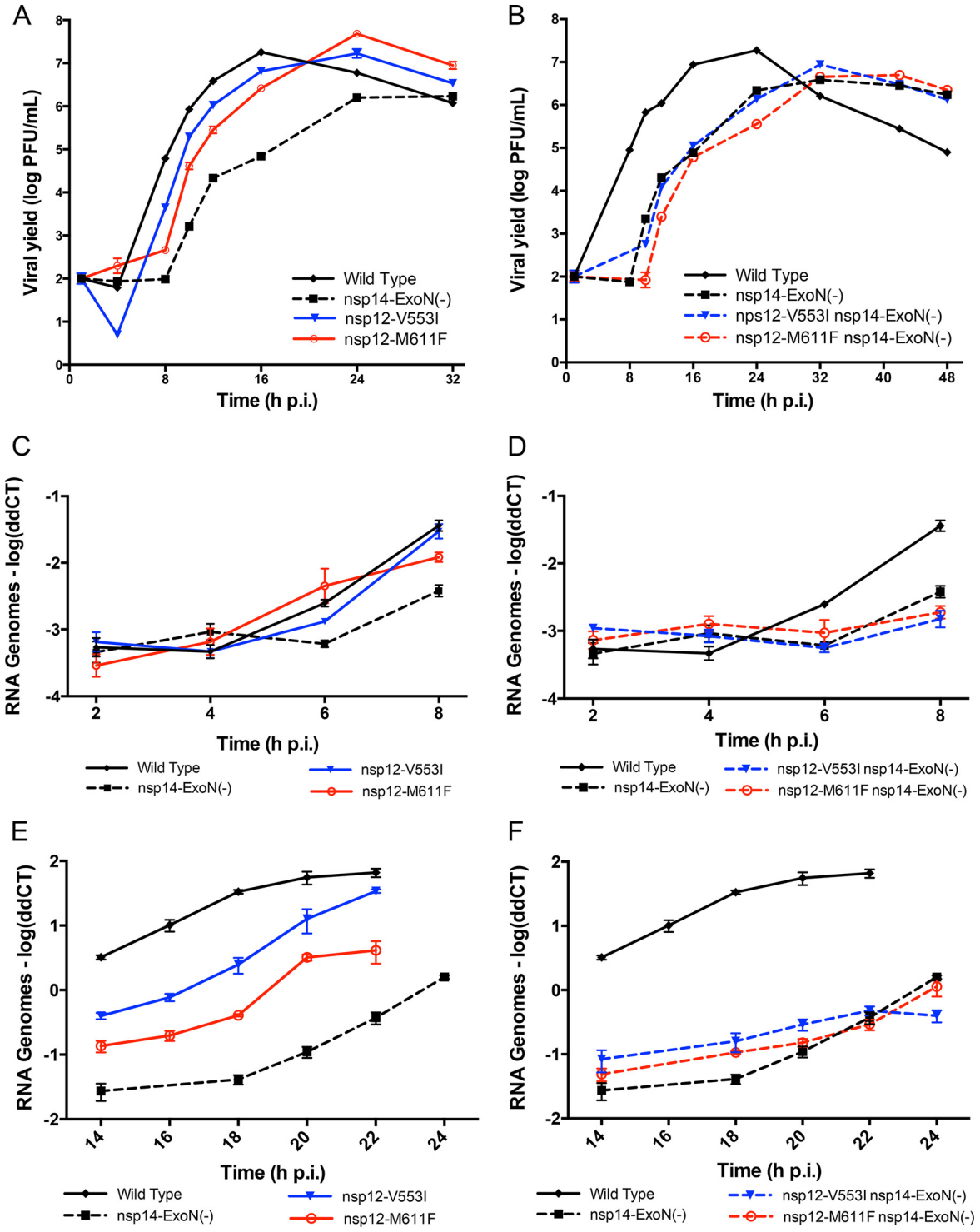

FIG 3 Replication kinetics of MHV nsp12-RdRp mutant viruses. The mutation location is indicated as follows: fingers, blues; palm, red. DBT cells were infected with the viruses indicated in the WT background (A, C, and E) or the nsp14-ExoN(−) background (B, D, and F) at an MOI of 0.01 PFU/cell. Supernatant aliquots were taken at the indicated times p.i., and titers were determined by plaque assay. Total RNA was taken at the indicated times p.i., and RT-qPCR was performed. The data represent the results of 3 independent experiments. The error bars represent SEM.

that of the WT. In contrast, in the nsp14-ExoN(−) background, both nsp12-V553I and nsp12-M611F mutant viruses displayed replication kinetics similar to those of the isogenic nsp14-ExoN(−) background. We also assessed RNA synthesis for nsp12-V553I and nsp12-M611F by RT-qPCR. The measured genomic-RNA levels were consistent with the virus replication kinetics data, and we observed delayed and decreased genome RNA synthesis in the WT background after multiple rounds of replication (Fig. 3E).

However, at early time points, there was no difference in RNA accumulation, suggesting that decreased RNA is a result of post-RNA synthesis steps (Fig. 3C). In the nsp14-ExoN(−) background, RNA synthesis levels were indistinguishable from the nsp14-ExoN(−) background for both nsp12-V553I and nsp12-M611F, with no additional RNA synthesis defects detectable (Fig. 3D and F). The results, along with the ability to recover several of the nsp12-RdRp mutants only in the nsp14-ExoN(+) background, support the hypothesis that nsp14-ExoN and nsp12-RdRp may have an epistatic relationship. However, for replication kinetics, the effects of nsp12-V553I and nsp12-M611F were not observable in the presence of inactive nsp14-ExoN, demonstrating that the replication phenotype of inactive nps14-ExoN is epistatic to replication variants encoded in nsp12-RdRp.

Specific infectivity of nsp12-V553I and nsp12-M611F. Having identified two mutant viruses with resistance to 5-FU, we wanted to further test whether the resistance was due to decreased incorporation of the mutagen. Measurement of specific infectivity has been useful for determining lethal mutagenesis for MHV and other RNA viruses (30, 56). We tested the nsp12-M611F and nsp12-V553I mutants in both the WT and nsp14-ExoN(−) backgrounds for changes in specific infectivity when infected at an MOI of 0.01 and treated with 5-FU (Fig. 4). Both nsp12-M611F and nsp12-V553I resulted in an increased ratio of infectious particles (PFU per milliliter) to total particles (RNA genomes) in the nsp14-ExoN(−) background (Fig. 4B). Similarly, in the WT background, nsp12-M611F demonstrated an increase in the ratio of infectious particles to RNA genomes (Fig. 4A). Thus, specific infectivity may be a more sensitive measure of lower-level changes in nucleotide selectivity in the setting of nsp14-ExoN(−).

Fitness costs of nsp12-V553I and nsp12-M611F in WT and nsp14-ExoN(−) backgrounds. In multiple RNA viruses, including CoVs, both increased and decreased fidelity have been reported to have a fitness cost (14). We therefore sought to determine whether nsp12-V553I or nsp12-M611F conferred any cost in fitness, defined as the ability to directly compete during coinfection. In the WT background, both nsp12-V553I and nsp12-M611F demonstrated delays in replication and impaired RNA accumulation. However, since there were no observed additional defects in replication or RNA synthesis for nsp12-V553I and nsp12-M611F when introduced into the nsp14-ExoN(−) background (Fig. 3B, D, and F), we tested for any additional fitness cost of nsp12-V553I/nsp14-ExoN(−) or nsp12-M611F/nsp14-ExoN(−) virus compared with nsp14-ExoN(−) alone. When coinfected with nsp14-ExoN(−) virus at ratios from 1:9 to 9:1, nsp12-V553I/nsp14-ExoN(−) maintained the input ratio compared with nsp14-ExoN(−) (Fig. 5A). A small advantage for nsp12-V553I/nsp14-ExoN(−) was observed when the coinfected cultures were treated with 60 μM 5-FU, consistent with a conferred advantage for 5-FU resistance (Fig. 5A). Thus, there appeared to be no additional fitness cost of nsp12-V553I/nsp14-ExoN(−) compared to nsp14-ExoN(−) alone. In contrast, nsp12-M611F/nsp14-ExoN(−) was not able to compete with nsp14-ExoN(−) at any ratio (Fig. 5B). Treatment with 60 μM 5-FU again favored nsp12-M611F/nsp14-ExoN(−); however, even then, the percentage of the population made up of nsp12-M611F/nsp14-ExoN(−) virus remained at only around 30% when initially given a 9-fold advantage (Fig. 5B).

We next tested whether the relative differences in fitness cost resulted in selective pressure for reversion of nsp12-V553I and nsp12-M611F (Fig. 6). DBT cells were infected with nsp12-V553I, nsp12-V553I/nsp14-ExoN(−), nsp12-M611F, or nsp12-M611F/nsp14-ExoN(−) virus at an initial MOI of 0.01. After 5 passages, the viruses were analyzed for retention of original mutations using dideoxy (Sanger) sequencing. The nsp12-V553I mutation was stable after passage in both WT and nsp14-ExoN(−) backgrounds, maintaining the mutated AUU codon (Fig. 6A), suggesting minimal selective pressure on that nucleotide, codon, or amino acid. In contrast, the nsp12-M611F mutation demonstrated significant change over passage in both the WT and the nsp14-ExoN(−) backgrounds. The original mutation, UUC, was no longer the majority codon in the nsp14-ExoN(−) background and was less than 52% of the population in all WT background lineages (Fig. 6B). The nsp12-M611F/nsp14-ExoN(−) population resulted in a mixture of 2-nucleotide changes, resulting in reversion to AUG (methionine) (≤68% of the population); single

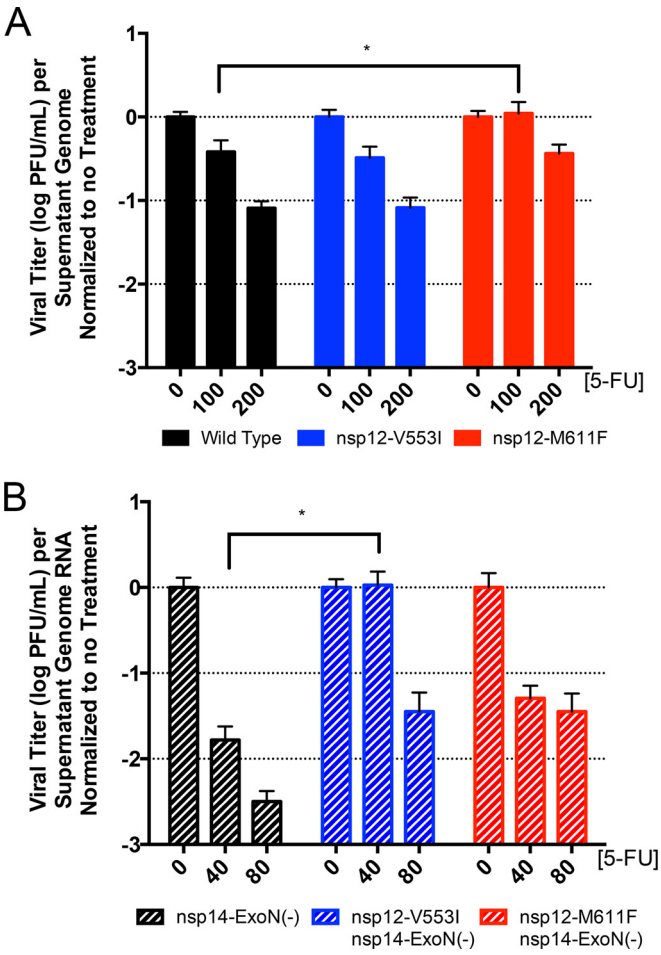

FIG 4 Specific infectivity is increased in both nsp12-V553I and nsp12-M611F mutants. DBT cells were pretreated with increasing concentrations of 5-FU for 30 min. The treatment was removed, and the cells were infected with the indicated viruses in the WT background (A) or the nsp14-ExoN(−) background (B) at an MOI of 0.01. The medium containing 5-FU was replaced 60 min p.i. Virus samples were taken at 20 and 24 h p.i. Titers were determined by plaque assay, and the numbers of supernatant genomes were determined using one-step RT-qPCR. The data represent the results of 2 independent experiments, each with 3 replicates. The error bars represent SEM (*, $P < 0.05$ by 2-way analysis of variance [ANOVA] using the Bonferroni correction for multiple comparisons).

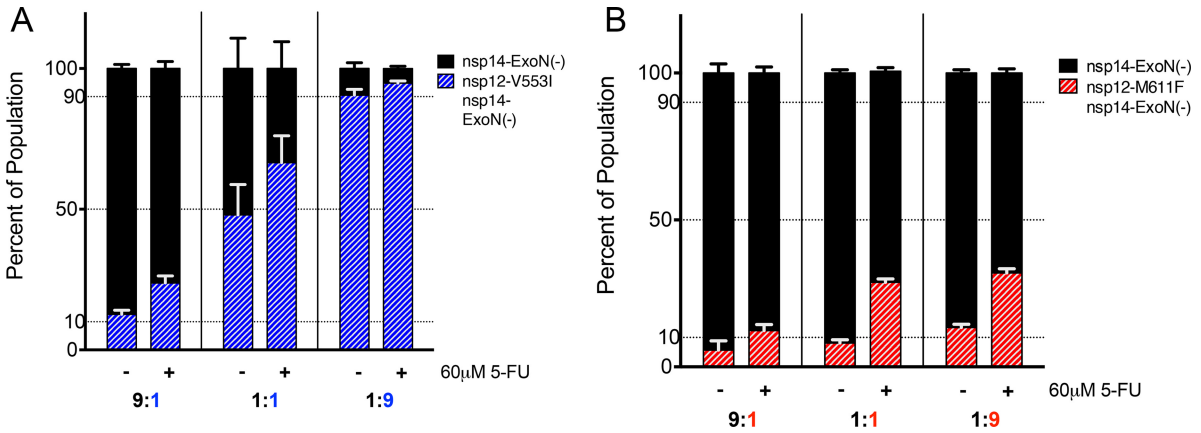

FIG 5 Competitive fitness analysis in the nsp14-ExoN(−) background. DBT cells were pretreated with medium alone or medium containing 60 μM 5-FU for 30 min. The treatment was removed, and the cells were coinfected at a total MOI of 0.01 with nsp14-ExoN(−) and nsp12-V553I/nsp14-ExoN(−) (A) or nsp12-M611F/nsp14-ExoN(−) (B) viruses at a ratio of 9:1, 1:1, or 1:9. Medium alone or containing 60 μM 5-FU was replaced 30 min p.i. Total RNA was taken at 24 h p.i. Sequencing was performed across a 1.7-kb region of nsp12-RdRp that included both mutations. The data represent the results of 3 independent experiments, each with 2 replicates. The error bars represent SEM.

nucleotide changes that resulted in mutation to Leu (≤55% of the population), a somewhat smaller but still hydrophobic residue; or retaining a Phe substitution (≤27% of the population). Thus, the fitness cost of nsp12-M611F results in significant selective pressure for changes at that residue during passage in the absence of 5-FU.

Resistance of recovered mutant viruses to the base analog 5-azacytidine. Having shown that both nsp12-M611F and nsp12-V553I mutations conferred resistance to 5-FU in the nsp14-ExoN(−) background but that nsp12-M611F reverted quickly and was at a fitness disadvantage in both the WT and nsp14-ExoN(−) backgrounds, we next wanted to test whether the mutations conferred resistance specifically to 5-FU or broadly to base analogs and therefore were likely determinants of fidelity. A study by Arias et al. demonstrated that for foot-and-mouth disease virus (FMDV), resistance to a specific mutagen can result from a point mutation while conferring the opposite overall fidelity (57). We therefore tested for resistance to the additional mutagen 5-AZC. Similar to the 5-FU results, the nsp12-V553I/nsp14-ExoN(−) mutant virus was more resistant to 5-AZC than nsp14-ExoN(−) alone, maintaining approximately 1-log-unit-higher titers from 20 to 50 μM 5-AZC (Fig. 7). However, the nsp12-M611F/nsp14-ExoN(−) mutant virus showed no difference in resistance to 5-AZC compared with nsp14-ExoN(−) alone (Fig. 7). These data suggest that nsp12-V553I is likely a fidelity determinant, whereas nsp12-M611F confers specific resistance to 5-FU and has unknown overall fidelity. This result is also consistent with the rapid reversion observed for the nsp12-M611F mutation.

The nsp12-V533I mutation results in a decrease in the accumulation of mutations. Having shown that the nsp12-V553I and nsp12-M611F mutations resulted in resistance to 5-FU and that nsp12-V553I additionally conferred resistance to 5-AZC, we sought to directly determine whether either of the mutations resulted in a change in the number of mutations accumulated in viral RNA. DBT cells were infected with wild-type, nsp12-V553I, nsp12-M611F, nsp14-ExoN(−), nsp12-V553I/nsp14-ExoN(−), or nsp12-M611F/nsp14-ExoN(−) virus at an MOI of 0.01, and RNA was collected at 20 h p.i. The samples were then prepared for Illumina next-generation sequencing (NGS) across the full genome and analyzed using the ViVan analysis pipeline (45). Mutations present at 1% or more of the population were graphed by frequency and position in the genome, with engineered mutations depicted with colored dots. Most nonengineered new mutations were present at 10% or less of the population and were distributed across the genome with no detectable hot spots (Fig. 8A to F). For nsp12-V553I in the WT background, no difference was observed in the number of mutations accumulated to 1% or greater of the population compared to the WT alone. In contrast, in the nsp14-ExoN(−) background, nsp12-V553I was associated with a 1.7-fold decrease in the frequency of mutations compared to nsp14-ExoN(−) alone (Fig. 8G), again with no change in the distribution of mutations across the genome (Fig. 8C and D). These results are consistent with both the 5-FU and 5-AZC data in suggesting increased fidelity. The results from the nsp12-M611F mutant viruses were more complicated. To our surprise, the nsp12-M611F/nsp14-ExoN(−) virus fully reverted at both engineered nsp12-M611F nucleotides during the low-MOI infection, resulting in a virus population that was nsp14-ExoN(−) alone (Fig. 8F). This reversion made the results for the nsp12-M611F/nsp14-ExoN(−) virus uninterpretable. However, since accumulation of mutations to over 1% of the population is a combination of all replication cycles from initial recovery to the final sample [roughly 11 in total for nsp12-M611F/nsp14-ExoN(−)], we included these data in Fig. 8G and H. In the WT background, the nsp12-M611F mutations were still present at 100% of the population and resulted in a 1.93-fold increase in the total number of accumulated mutations. We observed only a slight increase in the number of mutations accumulated in the nsp12-M611F/nsp14-ExoN(−) sample over those of nsp14-ExoN(−), which was not surprising, as the M611F mutation was no longer present. Neither sample appeared to have mutations concentrated in specific locations across the genome, suggesting the accumulation of mutations was due to random generation of mutations rather than strong selection in particular locations or proteins (Fig. 8E and F). Of note, one mutation in nsp3 of the nsp14-ExoN(−) sample and a mutation in the nsp3, nsp13, and E proteins of nsp12-V553I/nsp14-ExoN(−) reached nearly 100% of the sample population. None of these mutations were present in the fragments used for recovery, and the nsp3

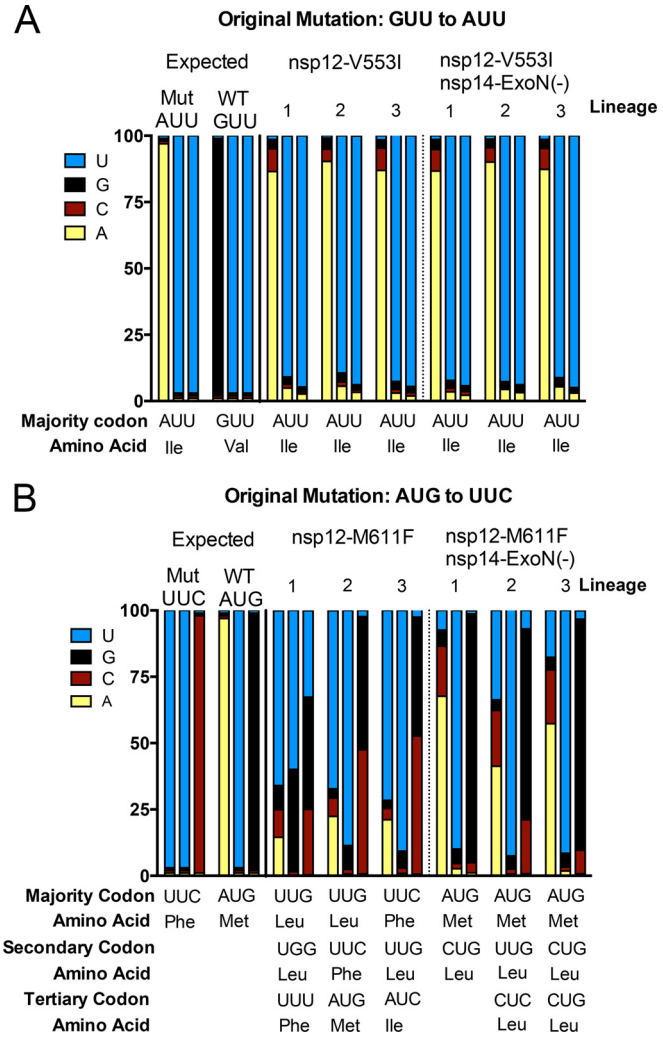

FIG 6 The nsp12-V553I mutation is stable across passages; however, nsp12-M611F is vulnerable to reversion. DBT cells were infected at an initial MOI of 0.01 and then blind passaged in triplicate for 5 passages. Total RNA was taken, and sequencing was performed across a 1.7-kb region of nsp12-RdRp that included both mutations. The percentage of each nucleotide present in each of the triplicate lineages after 5 passages is shown. Mutant viruses in the WT and nsp14-ExoN(−) backgrounds are shown. The original mutation for each of the viruses is shown above the graph, and the likely majority, secondary and tertiary codons present in the population are shown below the graph.

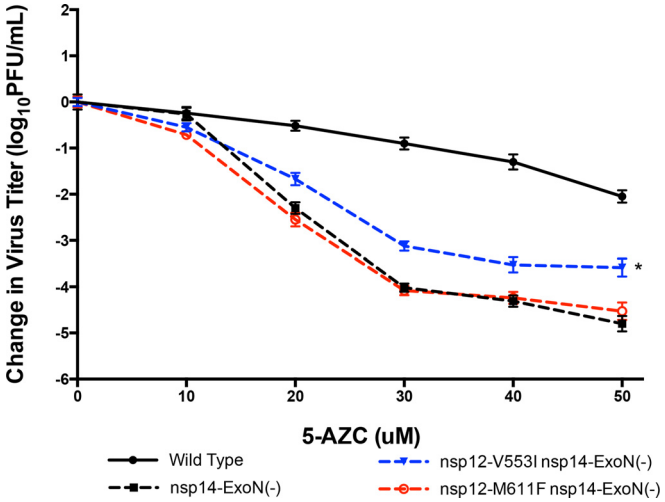

FIG 7 Resistance of MHV nsp12-RdRp V553I and M611F mutant viruses to 5-azacytidine in the nsp14-ExoN(−) background. The domain locations of mutations are indicated as follows: fingers, blues; palm, reds. DBT cells were pretreated with different concentrations of 5-AZC for 30 min. The treatment was removed, and the cells were infected with the indicated viruses at an MOI of 0.01. The medium containing 5-AZC was replaced 30 min p.i. Virus samples were taken at 32 h p.i., and the titer was determined by plaque assay. The data represent the results of 5 independent experiments, each with 2 replicates. The error bars represent SEM (*, $P < 0.05$ by ratio paired t test).

mutation that arose in the nsp14-ExoN(−) population was not present prior to the final low-MOI infection. It is possible that these mutations provided some benefit to the viruses, since they were fixed so rapidly in the population. We next determined whether either of the mutations resulted in a change in the types of mutations occurring during replication (Fig. 8H). Consistent with our previous studies, there were differences in the types of mutations incorporated when WT and nsp14-ExoN(−) backgrounds were compared (30). However, the addition of nsp12-V553I or nsp12-M611F did not alter these patterns in either the WT or nsp14-ExoN(−) background. Thus, nsp12-V553I results in an overall decrease in the accumulation of mutations over passages while nsp12-M611F seems to increase the number of mutations accumulated. These results confirm by sequence analysis the results from the 5-FU and 5-AZC resistance experiments for nsp12-V553I, specifically, showing that the effects of nsp12-V553I are dependent on inactivation of nsp14-ExoN for their detection and that nsp12-V553I likely confers broad resistance to the incorporation of incorrect nucleotides. In contrast, these results further increase the complexity of the nsp12-M611F mutation in relation to incorporation of nucleotides and their analogs. We conclude that nsp12-M611F confers resistance to 5-FU but that this resistance is not likely to be due to broad resistance to the incorporation of alternate nucleotides.

DISCUSSION

RdRp structures of divergent RNA viruses are structurally conserved and likely have common determinants of activity in the finger, palm, and thumb domains. Positive-strand RNA virus polymerases appear to utilize a common palm domain-based mechanism for active-site closure (23), and associated molecular determinants of fidelity in different RdRp domains have been proposed based on biochemical and mutagenesis studies (10). To date, there are no solved crystal structures of any CoV RdRp, and thus, direct comparison with other virus RdRp structures has not been possible. Further, regulation of CoV fidelity is likely dependent on multiple proteins, including the RdRp and proofreading ExoN. Thus, it was not clear that a CoV would phenotypically exhibit effects from mutating fidelity-determining residues located in the RdRp itself. In this study, we sought to determine whether we could use structure and mutagenesis data from distantly related RNA viruses to identify determinants of CoV nsp12-RdRp fidelity. Our results suggest that CoV RdRps do in fact participate in fidelity regulation at residues orthologous to those in the picornaviruses and likely in other RNA virus RdRps. The results also define, for the first time, a CoV RdRp determinant that increases resistance to multiple mutagens, decreases the accumulation of mutations over time, and so likely increases overall fidel-

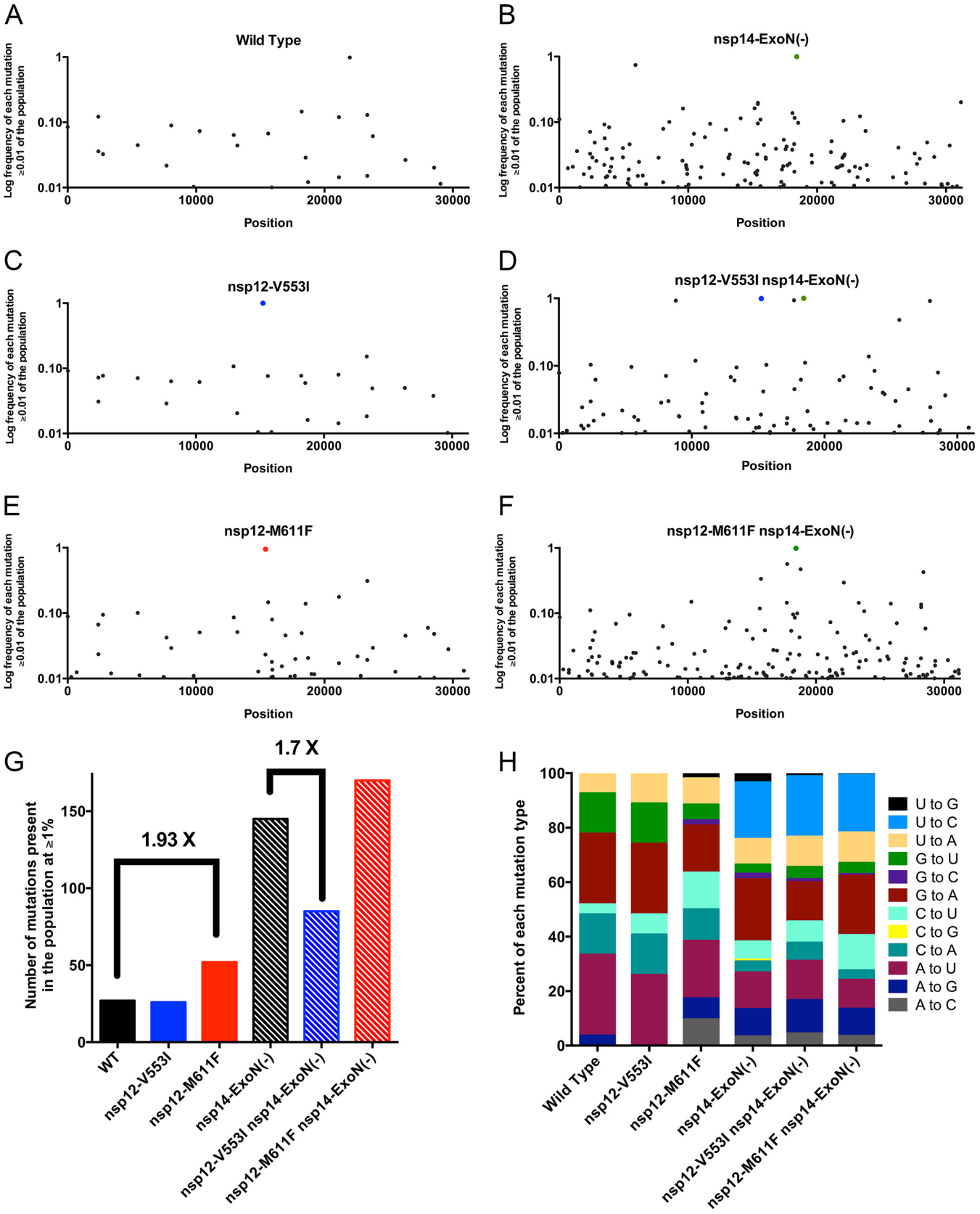

FIG 8 The nsp12-V553I mutation confers decreased accumulation of mutations in the nsp14-ExoN(−) background with no bias toward the exclusion of specific nucleotides. DBT cells were infected at an MOI of 0.01, and total RNA was collected. Deep sequencing was performed on the samples. The statistically significant mutations present at ≥1% of the total population are shown for the wild type, nsp14-ExoN, and nsp12-V553I or nsp12-M611F in both backgrounds. They are graphed according to their distribution across the genome (A to F), with intentionally introduced mutations shown with circles colored blue (nsp12-V553I), red (nsp12-M611F), or green [nsp14-ExoN(−)] (B to F); as the total number of mutations present in the population (G); and as the percentage of specific mutations present (H).

ity. Additionally, the data presented in this paper suggest that CoV RdRp-mediated increased fidelity is detectable only when nsp14-ExoN is inactive and only partially compensates for the loss of nsp14-ExoN high fidelity. Finally, both the nsp12-V553I and M611F mutations confer a replication cost in the WT background, but only nsp12-M611F confers a fitness disadvantage in the nsp14-ExoN(−) background. Together, the results suggest that nsp14-ExoN proofreading activity is epistatic to nsp12-RdRp fidelity but that in contrast, the replication defects of an inactive nsp14-ExoN are epistatic to replication defects in nsp12-RdRp.

Determinants of nucleotide selectivity and fidelity in CoVs may be conserved with other RNA viruses. Picornavirus functional RdRps contain only RdRp domains (58, 59). This is not the case for many viral RdRps, including CoVs (26, 39). In addition to the predicted RdRp core domain, all CoV nsp12 proteins contain a "CoV-specific" domain of over 350 amino acids at the N terminus of the protein. A nucleotidyltransferase activity was identified in this CoV-specific domain and has been shown to be important in SARS-CoV replication, but the specific function in replication remains to be determined (39). The N-terminal CoV-specific domain could not be modeled due to a lack of evolutionary homologues with known structures, but the predicted RdRp core domain could be modeled with high confidence using bioinformatic approaches. The structures that provided the best models for the CoV RdRp were from picornaviruses, including enterovirus 71, foot and mouth disease virus, and coxsackie virus B3. This allowed direct alignment and comparison of the known fidelity determinants in CVB3 with the MHV nsp12 core domain across both finger and palm domains. The recovery of mutations in these structurally conserved residues and their participation in CoV nucleotide selectivity support the hypothesis that there are determinants of base specificity conserved between CoVs and distantly related RNA viruses, specifically the picornaviruses. This supports the idea that all RdRps function similarly due to their structural conservation and despite the low level of sequence similarity and attached domains (54). It also suggests that the CoV RdRp domain folds in a manner similar to that of other RdRps, likely separate from the CoV-specific domain.

RdRp fidelity and nucleotide selectivity have been investigated extensively in picornaviruses, especially poliovirus (12, 15, 51, 53, 60, 61). However, even between picornaviruses, the impact on the fidelity of changes at identical or similar residues can vary dramatically (10). Mutations at the same residues in the RdRp of poliovirus and CVB3 affect fidelity differently; poliovirus mutations generally result in increased fidelity and CVB3 mutations in decreased fidelity (11). Specifically, the residue structurally orthologous to nsp12-M611 in poliovirus is F230, and in CVB3 it is I230; when F230 is mutated to Ile in poliovirus, it results in an increase in fidelity, but when I230 in CVB3 is mutated to Phe, Trp, or Val, it results in a decrease in fidelity (10). Similarly, the residue orthologous to nsp12-V553 in CVB3 is I176; when I176 is mutated to Val in CVB3, it results in a decrease in fidelity (10, 11). Although the specific substitutions differ, when nsp12-V553I and nsp12-M611F are introduced into the MHV genome, the resulting 5-FU resistance, and for nsp12-V553I a likely increase in fidelity, mimics results seen in poliovirus rather than CVB3. However, nsp12-M611F seemed to accumulate more mutations over time than controls, and many of the predicted mutations were recoverable only in the WT background; therefore, changes in nucleotide selectivity and fidelity were not tested, so it remains possible that the mutations that were nonviable in the nsp14-ExoN(−) background had decreased fidelity and that nsp14-ExoN(−) treated with 5-FU defines the error threshold for CoVs.

Coronavirus nsp12-RdRp and nsp14-ExoN cooperate to optimize both fidelity and replication kinetics. In addition to nsp12-RdRp, CoVs encode nsp14-ExoN, which functions as a proofreading enzyme (29, 30, 33, 35). Beyond nsp14-ExoN, there are additional CoV-encoded nsps that potentially contribute to overall fidelity, such as the small-molecule modulator of nsp14-ExoN encoded in nsp10 (33, 62), nsp7, and nsp8, which together function as an elongation factor (63) and a primase (64, 65), and nsp13, which functions as a helicase (66). These proteins interact with each other and likely function as a multiprotein replication-fidelity complex (34, 38). The results of this study show that while determinants in nsp12-RdRp are likely capable of increasing fidelity, the changes are detectable only in the setting of loss of nsp14-ExoN proofreading and do not completely compensate for the impaired fidelity associated with nsp14-ExoN(−). If altering nucleotide selectivity determinants within nsp12-RdRp no longer significantly affects the overall nucleotide selectivity of the WT virus, then the evolutionary pressure on nsp12-RdRp may be more heavily weighted toward other aspects of replication, such as speed. Recent evidence suggests that RdRp fidelity and speed have an inverse relationship (10, 67). Therefore, if fidelity regulation by nsp14-ExoN occurs more rapidly than correct nucleotide selectivity by the RdRp, then CoV nsp12-RdRp may have been selected specifically for replication speed. Our data may support this hypothesis, as in the WT background, both nsp12-V553I and nsp12-M611F resulted in increased replication lag phases (Fig. 3A and E), though early RNA synthesis was not observably different in our system (Fig. 3C). However, this was not seen in the nsp14-ExoN(−) background, which could be explained by our data indicating that replication is already slowed when nsp14-ExoN is inactivated. One possible mechanism for this could be that the nsp14-ExoN(−) protein is trying to remove incorrect nucleotides and is stalling replication due to its inability to do so. In this case, nsp14-ExoN(−) would be epistatic to nsp12-RdRp in relation to speed, thereby obscuring decreases in replication speed caused by mutations in nsp12-RdRp itself.

Conclusion. Our results support the hypothesis that determinants of nucleotide selectivity are conserved across viral orders, identify the first likely increased fidelity determinant for CoV nsp12-RdRp, and demonstrate that nsp14-ExoN proofreading activity is epistatic to nsp12-RdRp nucleotide selectivity. The possibility that some fidelity determinants may be conserved across viral orders is an exciting discovery, as many fidelity determinates identified so far have resulted in attenuation (11, 15, 54, 68–70). It would be interesting to determine whether nsp12-V553I is also attenuated. We predict that it is, based on the fitness cost *in vitro*. However, there is also no clear increase in nucleotide selectivity or fidelity in the WT background. This may be due to a very minimal change that is not measureable even with the deep-sequencing technology used in this study. Alternatively, it could be that any change is simply overwhelmed by the high fidelity of intact ExoN proofreading. In any case, these mutations or other changes at these residues may allow selection of viruses that replicate with normal kinetics *in vitro* and *in vivo* yet confer attenuation in an animal setting. We know that the nsp14-ExoN(−) mutations confer genotypically and phenotypically stable attenuation *in vivo* (36). However, the concept of a high-level mutator as a mecha-

nism for attenuation in live viruses may be problematic. The identification of increased fidelity mutations in the RdRp that can partially, or potentially completely, compensate for the fidelity impairment of nsp14-ExoN(−) viruses, may allow the development of approaches that can benefit from the stability of the nsp14-ExoN(−) mutator phenotype while allowing more stability to the input genomes. Finally, these results, combined with those from previous work (33, 44), suggest that CoVs encode at least three proteins involved in fidelity (nsp12-RdRp, nsp14-ExoN, and nsp10), supporting the assembly of a multiprotein replicase-fidelity complex, as described previously (38). This increases the importance of establishing a biochemical model of the multiprotein complex to directly test the interactions of fidelity determinants, as well as potential inhibitors of each or all of these functions.

ACKNOWLEDGMENTS

We thank Xiaotao Lu for technical assistance. We also thank James Brett Case and Erica Andres for critical reviews of the manuscript.

National Institutes of Health (NIH) grant R01 AI108197 (M.R.D.) provided support for this work. N.R.S. was supported by NIH Virology Training Program grant T32 AI089554. E.C.S. was supported by NIH Childhood Infection Research Program grant T32 AI095202. This work was also supported by the Elizabeth B. Lamb Center for Pediatric Research.

FUNDING INFORMATION

This work, including the efforts of Nicole Sexton, was funded by HHS | NIH | National Institute of Allergy and Infectious Diseases (NIAID) (T32 AI089554). This work, including the efforts of Everett Clinton Smith, was funded by HHS | NIH | National Institute of Allergy and Infectious Diseases (NIAID) (T32 AI095202). This work, including the efforts of Nicole Sexton, Everett Clinton Smith, and Mark R. Denison, was funded by HHS | NIH | National Institute of Allergy and Infectious Diseases (NIAID) (R01 AI10897).

REFERENCES

1. **Sanjuán R, Nebot MR, Chirico N, Mansky LM, Belshaw R.** 2010. Viral mutation rates. J Virol **84:**9733–9748. http://dx.doi.org/10.1128/JVI.00694-10.
2. **Crotty S, Cameron CE, Andino R.** 2001. RNA virus error catastrophe: direct molecular test by using ribavirin. Proc Natl Acad Sci U S A **98:**6895–6900. http://dx.doi.org/10.1073/pnas.111085598.
3. **Castro C, Arnold JJ, Cameron CE.** 2005. Incorporation fidelity of the viral RNA-dependent RNA polymerase: a kinetic, thermodynamic and structural perspective. Virus Res **107:**141–149. http://dx.doi.org/10.1016/j.virusres.2004.11.004.
4. **Schaaper RM.** 1993. Base selection, proofreading, and mismatch repair during DNA replication in Escherichia coli. J Biol Chem **268:**23762–23765.
5. **Smith EC, Denison MR.** 2012. Implications of altered replication fidelity on the evolution and pathogenesis of coronaviruses. Curr Opin Virol **2:**519–524. http://dx.doi.org/10.1016/j.coviro.2012.07.005.
6. **Sanjuán R.** 2012. From molecular genetics to phylodynamics: evolutionary relevance of mutation rates across viruses. Plos Pathog **8:**e1002685. http://dx.doi.org/10.1371/journal.ppat.1002685.
7. **Domingo E.** 2010. Mechanisms of viral emergence. Vet Res **41:**38. http://dx.doi.org/10.1051/vetres/2010010.
8. **Eigen M.** 1993. The origin of genetic information: viruses as models. Gene **135:**37–47. http://dx.doi.org/10.1016/0378-1119(93)90047-7.
9. **Arnold JJ, Vignuzzi M, Stone JK, Andino R, Cameron CE.** 2005. Remote site control of an active site fidelity checkpoint in a viral RNA-dependent RNA polymerase. J Biol Chem **280:**25706–25716. http://dx.doi.org/10.1074/jbc.M503444200.
10. **Campagnola G, McDonald S, Beaucourt S, Vignuzzi M, Peersen OB.** 2015. Structure-function relationships underlying the replication fidelity of viral RNA-dependent RNA polymerases. J Virol **89:**275–286. http://dx.doi.org/10.1128/JVI.01574-14.
11. **Gnädig NF, Beaucourt S, Campagnola G, Bordería AV, Sanz-Ramos M, Gong P, Blanc H, Peersen OB, Vignuzzi M.** 2012. Coxsackievirus B3 mutator strains are attenuated in vivo. Proc Natl Acad Sci U S A **109:**E2294–E2303. http://dx.doi.org/10.1073/pnas.1204022109.
12. **Vignuzzi M, Stone JK, Andino R.** 2005. Ribavirin and lethal mutagenesis of poliovirus: molecular mechanisms, resistance and biological implications. Virus Res **107:**173–181. http://dx.doi.org/10.1016/j.virusres.2004.11.007.
13. **Dapp MJ, Heineman RH, Mansky LM.** 2013. Interrelationship between HIV-1 fitness and mutation rate. J Mol Biol **425:**41–53. http://dx.doi.org/10.1016/j.jmb.2012.10.009.
14. **Smith EC, Sexton NR, Denison MR.** 2014. Thinking outside the triangle: replication fidelity of the largest RNA viruses. Annu Rev Virol **1:**111–132. http://dx.doi.org/10.1146/annurev-virology-031413-085507.
15. **Pfeiffer JK, Kirkegaard K.** 2005. Increased fidelity reduces poliovirus fitness and virulence under selective pressure in mice. Plos Pathog **1:**e11. http://dx.doi.org/10.1371/journal.ppat.0010011.
16. **Severson WE, Schmaljohn CS, Javadian A, Jonsson CB.** 2003. Ribavirin causes error catastrophe during Hantaan virus replication. J Virol **77:**481–488. http://dx.doi.org/10.1128/JVI.77.1.481-488.2003.
17. **Bruenn JA.** 2003. A structural and primary sequence comparison of the viral RNA-dependent RNA polymerases. Nucleic Acids Res **31:**1821–1829. http://dx.doi.org/10.1093/nar/gkg277.
18. **Lang DM, Zemla AT, Zhou CLE.** 2013. Highly similar structural frames link the template tunnel and NTP entry tunnel to the exterior surface in RNA-dependent RNA polymerases. Nucleic Acids Res **41:**1464–1482. http://dx.doi.org/10.1093/nar/gks1251.
19. **Butcher SJ, Grimes JM, Makeyev EV, Bamford DH, Stuart DI.** 2001. A mechanism for initiating RNA-dependent RNA polymerization. Nature **410:**235–240. http://dx.doi.org/10.1038/35065653.
20. **Ng KKS, Arnold JJ, Cameron CE.** 2008. Structure-function relationships among RNA-dependent RNA polymerases. Curr Top Microbiol Immunol **320:**137–156.
21. **Ferrer-Orta C, Arias A, Perez-Luque R, Escarmis C, Domingo E, Verdaguer N.** 2007. Sequential structures provide insights into the fidelity of RNA replication. Proc Natl Acad Sci U S A **104:**9463–9468. http://dx.doi.org/10.1073/pnas.0700518104.
22. **Ferrer-Orta C, Ferrero D, Verdaguer N.** 2015. RNA-dependent RNA polymerases of picornaviruses: from the structure to regulatory mechanisms. Viruses **7:**4438–4460. http://dx.doi.org/10.3390/v7082829.
23. **Gong P, Peersen OB.** 2010. Structural basis for active site closure by the poliovirus RNA-dependent RNA polymerase. Proc Natl Acad Sci U S A **107:**22505–22510. http://dx.doi.org/10.1073/pnas.1007626107.
24. **Brockway SM, Clay CT, Lu XT, Denison MR.** 2003. Characterization of the expression, intracellular localization, and replication complex association of the putative mouse hepatitis virus RNA-dependent RNA polymerase. J Virol **77:**10515–10527. http://dx.doi.org/10.1128/JVI.77.19.10515-10527.2003.
25. **Nagy PD, Barajas D, Pogany J.** 2012. Host factors with regulatory roles in tombusvirus replication. Curr Opin Virol **2:**691–698. http://dx.doi.org/10.1016/j.coviro.2012.10.004.
26. **te Velthuis AJW.** 2014. Common and unique features of viral RNA-dependent polymerases. Cell Mol Life Sci **71:**4403–4420. http://dx.doi.org/10.1007/s00018-014-1695-z.
27. **Peiris JSM, Lai ST, Poon LLM, Guan Y, Yam LYC, Lim W, Nicholls J, Yee WKS, Yan WW, Cheung MT, Cheng VCC, Chan KH, Tsang DNC, Yung RWH, Ng TK, Yuen KY, SARS Study Group.** 2003. Coronavirus as a possible cause of severe acute respiratory syndrome. Lancet **361:**1319–1325. http://dx.doi.org/10.1016/S0140-6736(03)13077-2.
28. **Zaki AM, van Boheemen S, Bestebroer TM, Osterhaus ADME, Fouchier RAM.** 2012. Isolation of a novel coronavirus from a man with pneumonia in Saudi Arabia. N Engl J Med **367:**1814–1820. http://dx.doi.org/10.1056/NEJMoa1211721.
29. **Eckerle LD, Becker MM, Halpin RA, Li K, Venter E, Lu X, Scherbakova S, Graham RL, Baric RS, Stockwell TB, Spiro DJ, Denison MR.** 2010. Infidelity of SARS-CoV Nsp14-exonuclease mutant virus replication is revealed by complete genome sequencing. Plos Pathog **6:**e1000896. http://dx.doi.org/10.1371/journal.ppat.1000896.
30. **Smith EC, Blanc H, Vignuzzi M, Denison MR.** 2013. Coronaviruses lacking exoribonuclease activity are susceptible to lethal mutagenesis: ev-

idence for proofreading and potential therapeutics. Plos Pathog **9:**e1003565. http://dx.doi.org/10.1371/journal.ppat.1003565.
31. **Gorbalenya AE, Enjuanes L, Ziebuhr J, Snijder EJ.** 2006. Nidovirales: evolving the largest RNA virus genome. Virus Res **117:**17–37. http://dx.doi.org/10.1016/j.virusres.2006.01.017.
32. **Stenglein MD, Jacobson ER, Wozniak EJ, Wellehan JFX, Kincaid A, Gordon M, Porter BF, Baumgartner W, Stahl S, Kelley K, Towner JS, Derisi JL.** 2014. Ball python nidovirus: a candidate etiologic agent for severe respiratory disease in Python regius. mBio **5:**e01484–14. http://dx.doi.org/10.1128/mBio.01484-14.
33. **Bouvet M, Imbert I, Subissi L, Gluais L, Canard B, Decroly E.** 2012. RNA 3′-end mismatch excision by the severe acute respiratory syndrome coronavirus nonstructural protein nsp10/nsp14 exoribonuclease complex. Proc Natl Acad Sci U S A **109:**9372–9377. http://dx.doi.org/10.1073/pnas.1201130109.
34. **Smith EC, Denison MR.** 2013. Coronaviruses as DNA wannabes: a new model for the regulation of RNA virus replication fidelity. Plos Pathog **9:**e1003760. http://dx.doi.org/10.1371/journal.ppat.1003760.
35. **Eckerle LD, Lu X, Sperry SM, Choi L, Denison MR.** 2007. High fidelity of murine hepatitis virus replication is decreased in nsp14 exoribonuclease mutants. J Virol **81:**12135–12144. http://dx.doi.org/10.1128/JVI.01296-07.
36. **Graham RL, Becker MM, Eckerle LD, Bolles M, Denison MR, Baric RS.** 2012. A live, impaired-fidelity coronavirus vaccine protects in an aged, immunocompromised mouse model of lethal disease. Nat Med **18:**1820–1826. http://dx.doi.org/10.1038/nm.2972.
37. **Denison MR, Graham RL, Donaldson EF, Eckerle LD, Baric RS.** 2011. Coronaviruses: an RNA proofreading machine regulates replication fidelity and diversity. RNA Biol **8:**270–279. http://dx.doi.org/10.4161/rna.8.2.15013.
38. **Subissi L, Posthuma CC, Collet A, Zevenhoven-Dobbe JC, Gorbalenya AE, Decroly E, Snijder EJ, Canard B, Imbert I.** 2014. One severe acute respiratory syndrome coronavirus protein complex integrates processive RNA polymerase and exonuclease activities. Proc Natl Acad Sci U S A **111:**E3900–E3909. http://dx.doi.org/10.1073/pnas.1323705111.
39. **Lehmann KC, Gulyaeva A, Zevenhoven-Dobbe JC, Janssen GMC, Ruben M, Overkleeft HS, van Veelen PA, Samborskiy DV, Kravchenko AA, Leontovich AM, Sidorov IA, Snijder EJ, Posthuma CC, Gorbalenya AE.** 2015. Discovery of an essential nucleotidylating activity associated with a newly delineated conserved domain in the RNA polymerase-containing protein of all nidoviruses. Nucleic Acids Res **43:**8416–8434. http://dx.doi.org/10.1093/nar/gkv838.
40. **Xu X, Liu Y, Weiss S, Arnold E, Sarafianos SG, Ding J.** 2003. Molecular model of SARS coronavirus polymerase: implications for biochemical functions and drug design. Nucleic Acids Res **31:**7117–7130. http://dx.doi.org/10.1093/nar/gkg916.
41. **Chen W, Baric RS.** 1996. Molecular anatomy of mouse hepatitis virus persistence: coevolution of increased host cell resistance and virus virulence. J Virol **70:**3947–3960.
42. **Yount B, Denison MR, Weiss SR, Baric RS.** 2002. Systematic assembly of a full-length infectious cDNA of mouse hepatitis virus strain A59. J Virol **76:**11065–11078. http://dx.doi.org/10.1128/JVI.76.21.11065-11078.2002.
43. **Kelley LA, Mezulis S, Yates CM, Wass MN, Sternberg MJE.** 2015. The Phyre2 Web portal for protein modeling, prediction and analysis. Nat Protoc **10:**845–858. http://dx.doi.org/10.1038/nprot.2015.053.
44. **Smith EC, Case JB, Blanc H, Isakov O, Shomron N, Vignuzzi M, Denison MR.** 2015. Mutations in coronavirus nonstructural protein 10 decrease virus replication fidelity. J Virol **89:**6418–6426. http://dx.doi.org/10.1128/JVI.00110-15.
45. **Isakov O, Bordería AV, Golan D, Hamenahem A, Celniker G, Yoffe L, Blanc H, Vignuzzi M, Shomron N.** 2015. Deep sequencing analysis of viral infection and evolution allows rapid and detailed characterization of viral mutant spectrum. Bioinformatics **31:**2141–2150. http://dx.doi.org/10.1093/bioinformatics/btv101.
46. **Li H, Durbin R.** 2010. Fast and accurate long-read alignment with Burrows-Wheeler transform. Bioinformatics **26:**589–595. http://dx.doi.org/10.1093/bioinformatics/btp698.
47. **Li H, Handsaker B, Wysoker A, Fennell T, Ruan J, Homer N, Marth G, Abecasis G, Durbin R, 1000 Genome Project Data Processing Subgroup.** 2009. The sequence alignment/map format and SAMtools. Bioinformatics **25:**2078–2079.
48. **Bordería AV, Isakov O, Moratorio G, Henningsson R, Agüera-González S, Organtini L, Gnädig NF, Blanc H, Alcover A, Hafenstein S, Fontes M, Shomron N, Vignuzzi M.** 2015. Group selection and contribution of minority variants during virus adaptation determines virus fitness and phenotype. Plos Pathog **11:**e1004838. http://dx.doi.org/10.1371/journal.ppat.1004838.
49. **Pauly MD, Lauring AS.** 2015. Effective lethal mutagenesis of influenza virus by three nucleoside analogs. J Virol **89:**3584–3597. http://dx.doi.org/10.1128/JVI.03483-14.
50. **Van Slyke GA, Arnold JJ, Lugo AJ, Griesemer SB, Moustafa IM, Kramer LD, Cameron CE, Ciota AT.** 2015. Sequence-specific fidelity alterations associated with West Nile virus attenuation in mosquitoes. Plos Pathog **11:**e1005009. http://dx.doi.org/10.1371/journal.ppat.1005009.
51. **Verdaguer N, Ferrer-Orta C.** 2012. Conformational changes in motif D of RdRPs as fidelity determinant. Structure **20:**1448–1450. http://dx.doi.org/10.1016/j.str.2012.08.014.
52. **Levi LI, Gnädig NF, Beaucourt S, McPherson MJ, Baron B, Arnold JJ, Vignuzzi M.** 2010. Fidelity variants of RNA dependent RNA polymerases uncover an indirect, mutagenic activity of amiloride compounds. Plos Pathog **6:**e1001163. http://dx.doi.org/10.1371/journal.ppat.1001163.
53. **Pfeiffer JK, Kirkegaard K.** 2003. A single mutation in poliovirus RNA-dependent RNA polymerase confers resistance to mutagenic nucleotide analogs via increased fidelity. Proc Natl Acad Sci U S A **100:**7289. http://dx.doi.org/10.1073/pnas.1232294100.
54. **Yang X, Smidansky ED, Maksimchuk KR, Lum D, Welch JL, Arnold JJ, Cameron CE, Boehr DD.** 2012. Motif D of viral RNA-dependent RNA polymerases determines efficiency and fidelity of nucleotide addition. Structure **20:**1519–1527. http://dx.doi.org/10.1016/j.str.2012.06.012.
55. **Holland JJ, Domingo E, de la Torre JC, Steinhauer DA.** 1990. Mutation frequencies at defined single codon sites in vesicular stomatitis virus and poliovirus can be increased only slightly by chemical mutagenesis. J Virol **64:**3960–3962.
56. **Rozen-Gagnon K, Stapleford KA, Mongelli V, Blanc H, Failloux A-B, Saleh M-C, Vignuzzi M.** 2014. Alphavirus mutator variants present host-specific defects and attenuation in mammalian and insect models. Plos Pathog **10:**e1003877. http://dx.doi.org/10.1371/journal.ppat.1003877.
57. **Arias A, Arnold JJ, Sierra M, Smidansky ED, Domingo E, Cameron CE.** 2008. Determinants of RNA-dependent RNA polymerase (in)fidelity revealed by kinetic analysis of the polymerase encoded by a foot-and-mouth disease virus mutant with reduced sensitivity to ribavirin. J Virol **82:**12346–12355. http://dx.doi.org/10.1128/JVI.01297-08.
58. **Hansen JL, Long AM, Schultz SC.** 1997. Structure of the RNA-dependent RNA polymerase of poliovirus. Structure **5:**1109–1122. http://dx.doi.org/10.1016/S0969-2126(97)00261-X.
59. **Campagnola G, Weygandt M, Scoggin K, Peersen O.** 2008. Crystal structure of coxsackievirus B3 3Dpol highlights the functional importance of residue 5 in picornavirus polymerases. J Virol **82:**9458–9464. http://dx.doi.org/10.1128/JVI.00647-08.
60. **Hobdey SE, Kempf BJ, Steil BP, Barton DJ, Peersen OB.** 2010. Poliovirus polymerase residue 5 plays a critical role in elongation complex stability. J Virol **84:**8072–8084. http://dx.doi.org/10.1128/JVI.02147-09.
61. **Korneeva VS, Cameron CE.** 2007. Structure-function relationships of the viral RNA-dependent RNA polymerase: fidelity, replication speed, and initiation mechanism determined by a residue in the ribose-binding pocket. J Biol Chem **282:**16135–16145. http://dx.doi.org/10.1074/jbc.M610090200.
62. **Chen Y, Su C, Ke M, Jin X, Xu L, Zhang Z, Wu A, Sun Y, Yang Z, Tien P, Ahola T, Liang Y, Liu X, Guo D.** 2011. Biochemical and structural insights into the mechanisms of SARS coronavirus RNA ribose 2′-O-methylation by nsp16/nsp10 protein complex. Plos Pathog **7:**e1002294. http://dx.doi.org/10.1371/journal.ppat.1002294.
63. **te Velthuis AJW, van den Worm SHE, Snijder EJ.** 2012. The SARS-coronavirus nsp7+nsp8 complex is a unique multimeric RNA polymerase capable of both de novo initiation and primer extension. Nucleic Acids Res **40:**1737–1747. http://dx.doi.org/10.1093/nar/gkr893.
64. **Imbert I, Guillemot J-C, Bourhis J-M, Bussetta C, Coutard B, Egloff M-P, Ferron F, Gorbalenya AE, Canard B.** 2006. A second, non-canonical RNA-dependent RNA polymerase in SARS coronavirus. EMBO J **25:**4933–4942. http://dx.doi.org/10.1038/sj.emboj.7601368.
65. **Xiao Y, Ma Q, Restle T, Shang W, Svergun DI, Ponnusamy R, Sczakiel G, Hilgenfeld R.** 2012. Nonstructural proteins 7 and 8 of feline coronavirus form a 2:1 heterotrimer that exhibits primer-independent RNA polymerase activity. J Virol **86:**4444–4454. http://dx.doi.org/10.1128/JVI.06635-11.

66. **Adedeji AO, Marchand B, te Velthuis AJW, Snijder EJ, Weiss S, Eoff RL, Singh K, Sarafianos SG.** 2012. Mechanism of nucleic acid unwinding by SARS-CoV helicase. PLoS One **7:**e36521. http://dx.doi.org/10.1371/journal.pone.0036521.
67. **Regoes RR, Hamblin S, Tanaka MM.** 2013. Viral mutation rates: modelling the roles of within-host viral dynamics and the trade-off between replication fidelity and speed. Proc Biol Sci **280:**20122047. http://dx.doi.org/10.1098/rspb.2012.2047.
68. **Vignuzzi M, Wendt E, Andino R.** 2008. Engineering attenuated virus vaccines by controlling replication fidelity. Nat Med **14:**154–161. http://dx.doi.org/10.1038/nm1726.
69. **Lauring AS, Jones JO, Andino R.** 2010. Rationalizing the development of live attenuated virus vaccines. Nat Biotechnol **28:**573–579. http://dx.doi.org/10.1038/nbt.1635.
70. **Coffey LL, Beeharry Y, Borderia AV, Blanc H, Vignuzzi M.** 2011. Arbovirus high fidelity variant loses fitness in mosquitoes and mice. Proc Natl Acad Sci U S A **108:**16038–16043. http://dx.doi.org/10.1073/pnas.1111650108.